Analysis and Simulation of LoRaWAN LR-FHSS for Direct-to-Satellite Scenario

Muhammad Asad Ullah, *Graduate Student Member, IEEE*, Konstantin Mikhaylov, *Senior Member, IEEE*, and Hirley Alves, *Member, IEEE*

***Abstract*—Long Range-Frequency Hopping Spread Spectrum (LR-FHSS) has been recently introduced into the LoRaWAN protocol specification to increase network capacity and collision robustness, and enable direct connectivity between machine devices and the Low Earth Orbit (LEO) satellites. In this letter, we first construct the analytical and simulation models for packet delivery over LR-FHSS from ground nodes to a LEO satellite, and then use the developed analytic and simulation models to generate the numerical results. Our results reveal the potential feasibility of large-scale networks, demonstrate some trade-offs between the two new LR-FHSS-based data rates for the EU region, and reveal the key reasons for packet losses.**

***Index Terms*—LR-FHSS, mMTC, LoRaWAN, LEO, satellites.**

I. Introduction

THE RECENT years have witnessed a significant progress for low-power wide-area networks (LPWAN) technologies, which open the doors for digitization all across the globe. Under the umbrella of LPWAN, Long-Range Wide Area Network (LoRaWAN) technology has become excessively widely used due to its promise of long-range connectivity, operation in license-exempt bands, and low energy consumption. To further advance LoRaWAN and enable support of satellite-based services, in the most recent version of the specification [1] LoRa Alliance has introduced the Long Range-Frequency Hopping Spread Spectrum (LR-FHSS) data rates (DRs).

The information about the LR-FHSS is still somewhat scarce, but the scheme promises high robustness against the co-channel interference through increasing spectral efficiency, and introducing coding and physical headers' redundancy. To transmit an LR-FHSS packet, an end-device (ED) splits the data into 233 ms long $N = 1, \ldots, 4$ headers and several fragments of 50 ms, and pushes them through the randomly selected frequency channels. Note that LR-FHSS can co-exist with the LoRa modulation without modifying the existing LoRaWAN network architecture. To leverage this incorporation, a single Adaptive Data Rate (ADR) command from the network server is sufficient to switch between the modulations [2].

The key purpose of LR-FHSS is to fill the connectivity gaps existing in the remote areas, where no terrestrial infrastructure is available. Specifically, the statistic reveals that only 10% of the Earth surface benefits from terrestrial connectivity due to geographical, economic and practical limitations. Therefore, to tackle this challenge, Academia and Industry consider satellite and Non-Terrestrial Networks (NTNs) for offering seamless Massive Machine Type Connectivity (mMTC) in remote areas [3], [4]. Specifically, the concept of combining LoRaWAN and the Low Earth Orbit (LEO) satellites has recently emerged in the research community.

To give an example, the studies [5] and [6] shed some light on state-of-the-art LPWAN technologies, network architectures, and existing protocols for direct-to-satellite (DtS) IoT, and highlighted LoRa as a prominent technology towards satellite IoT applications in remote areas. Similarly, in [7] and [8] the results obtained through extensive simulations reveal that LoRa and LEO satellite integration are promising for enabling mMTC applications in remote areas. Notably, these studies reveal that performance of LoRa-based DtS degrades primarily due to same-channel and same-spreading factor (SF) interference rather than the propagation-related losses. Furthermore, recently Lacuna Space has launched five LEO satellites with non-terrestrial LoRaWAN gateway orbiting at 500 km. The real-life trials demonstrated the feasibility of packet reception. Note that since LR-FHSS intends to support large-scale networks offering high robustness to interference, LoRaWAN-over-Satellite connectivity could become even more reliable with LR-FHSS owing to higher spectral efficiency, headers' replications and lower coding.

In [9], an initial insight into the performance of LR-FHSS has been provided and the results revealing potential of LR-FHSS to handle million of uplink packets a day have been reported. However, this letter (i) did not model the specifics of ground-to-satellite connectivity (e.g., channel), and (ii) reported only the results obtained from simulations for one specific scenario.

Therefore, in this letter, we investigate the potential feasibility and performance of LEO satellite and LoRaWAN integration, implying novel LR-FHSS modulation. The contribution of this letter is, thus, two-fold. First, we deliver to the research community both analytical and simulation models describing the performance of LR-FHSS modulation. Second, we use the developed models to obtain numerical results illustrating the performance of the LoRaWAN-over-satellite featuring LR-FHSS and providing some insights into the reasons of packet losses for two data rates defined for the EU region.

The rest of this letter is organized as follows. We summarize the background and key features of LR-FHSS in Section II. System model implications, and the developed

Manuscript received November 3, 2021; accepted December 7, 2021. Date of publication December 16, 2021; date of current version March 9, 2022. The associate editor coordinating the review of this article and approving it for publication was T. De Cola. *(Corresponding author: Muhammad Asad Ullah.)*

The authors are with the Centre for Wireless Communications, University of Oulu, 90570 Oulu, Finland (e-mail: muhammad.asadullah@oulu.fi).

Digital Object Identifier 10.1109/LWC.2021.3135984

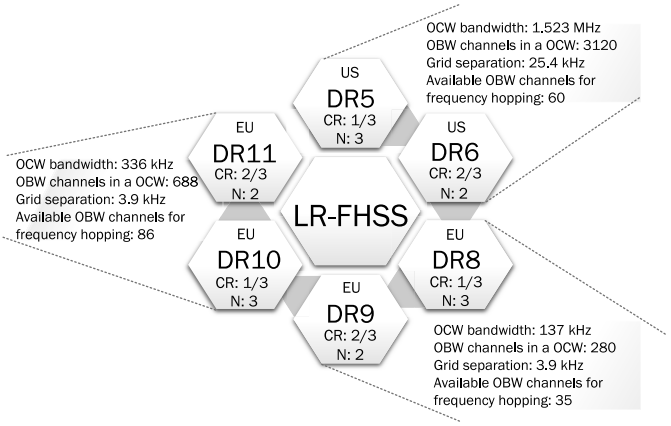

Fig. 1. Key parameters of LR-FHSS data rates for ETSI and FCC regions.

analytic and simulation models are detailed in Section III. Next, in Section IV we introduce the key parameters, present and discuss the numerical results. Finally, in Section V we summarize the key findings and point out some potential future research directions.

II. LR-FHSS Basics

First of all, we have to note that the open technical information about the LR-FHSS is today limited and can be obtained from the three primary documents: the RP2-1.0.2 LoRaWAN Regional Parameters [1], an overview paper [9] and Semtech blog post [2]. In what follows we summarize the key aspects of LR-FHSS, relevant for its analyzing, based on these sources.

The LR-FHSS implements a variant of frequency-hopping spread spectrum (FHSS) modulation. The whole frequency band is divided into Operating Channel Width (OCW) channels, bandwidth of which differs depending on the local frequency regulations as discussed in [1] and illustrated in Fig. 1. A single LR-FHSS OCW channel is further subdivided into multiple physical frequency channels with a bandwidth of 488 Hz, named Occupied Band Width (OBW) channels. At any moment of time a single end-device can transmit its data only in one OBW channel. The key parameters for the different regions are summarized in Fig. 1. Note that, in what follows we focus on LR-FHSS operating in the EU region, unless stated otherwise. However, our developed analytical and simulator models can be adapted for other regions as well.

Figure 2 illustrates the packet structure of LR-FHSS at the physical layer (PHY). For uplink communication, an LR-FHSS-based end-device initiates the transmission by sending N, $N = 1, \ldots, 4$ copies of the 0.233 ms-long header, using a new randomly-selected carrier frequency for each replication. Then, the L bytes of the PHY payload and cyclic redundancy check (CRC) are broken into fragments with the maximum duration of 50 ms and sent sequentially in the OBW frequency channels, which are picked by a Pseudorandom number generator (PRNG) [1], [9]. Note, that the specification prescribes upkeeping the minimum separation of 3.9 kHz between the channels used for transmitting sequential fragments. Under these implications, as summarized in Fig. 1, the new LoRaWAN data rates DR8 and DR9 allow an end-device

N (1 to 4) PHY header replicas				Once	
4 bytes	4 bytes	1 byte	2 bits	L bytes	2 bytes
SyncWord	PHDR	PHDR_CRC		PHYPayload	CRC

PHDR								
8 bits	3 bits	2 bits	1 bit	1 bit	4 bit	9 bit	2 bits	2 bits
Payload length	Data rate	Coding rate	Grid	Hop	Bandwidth	Hopping sequence	SyncWord index	RFU

Fig. 2. LR-FHSS physical layer packet structure.

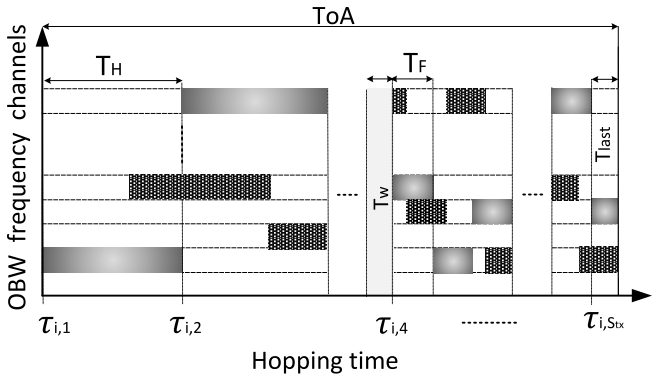

Fig. 3. Simultaneous transmission of two end-devices following LR-FHSS scheme.

to leverage 35 OBW physical channels inside a 137 kHz OCW channel. Conversely, DR10 and DR11 offer 86 OBW physical channels while using a 336 kHz OCW spectrum.

Note that DR8 and DR10 imply coding with the rate CR $= \frac{1}{3}$, thus adding some redundancy but improving the gateway's ability to correctly decode the packet even if several payload data fragments are lost. To fight the possibility of header loss, it is replicated $N = 3$ times. Meanwhile, DR9 and DR11 imply CR $= \frac{2}{3}$ and transmission of the header twice. Departing from the available information in [1], the overall on-air time of a LR-FHSS packet for L bytes physical layer payload can be expressed as

$$T_{air} = NT_H + T_W + 0.102\left\lceil \frac{L+2}{M} \right\rceil, \tag{1}$$

where $T_H = 233$ ms, M equals 2 and 4 for DR8/DR10 and DR9/DR11, respectively. T_W denotes a 2 bits delay intended to give a gateway enough time to process the headers, as illustrated in Fig. 2. During the transmission of the payload, an end-device randomly switches the OBW channels after every 50 ms, as illustrated in Fig. 3. Thus, the total number of the frequency hops S_{tx} is sum of headers and payload fragments which can be defined as [1]:

$$S_{tx} = N + \left\lceil \frac{0.102\left\lceil \frac{L+2}{M} \right\rceil}{T_F} \right\rceil, \tag{2}$$

where $T_F = 50$ ms is the hop period while sending the payload.

During LR-FHSS packet reception at the gateway, an outage occurs if either of the two conditions are satisfied; (i) all the N replicas of the header are lost, or (ii) the number of received data fragments is less than the pre-defined reception threshold

(γ). In other words, if more than $\frac{1}{3}$ (or $\frac{2}{3}$) of the physical payload fragments are lost, the payload reception will fail [9].

III. System Models

In the following subsections we start by discussing our system and propagation/collisions models, and then introduce our developed analytical model and detail our simulator. Unlike [9], we imply a LoRaWAN gateway deployed on an LEO satellite, which has orbital characteristics similar to that of Iridium satellites. A single gateway equipped with an antenna array serves up to $\mathcal{N} = 50,000$ nodes, unless stated otherwise, which are uniformly distributed within a circular area of 15,299,900 km^2, which equates to a satellite's footprint radius of $r = 2209$ km. We consider each node generating $Q = 4$ uplink packets at random times during the interval of an hour ($D = 3600$ s) and broadcasting them.

A. Analytic Model

The interval (0; D) is divided exponentially by $n = \mathcal{N} \times Q \times S_{tx}$ packet element arrivals with the average interarrival time $\mu = \frac{D}{\mathcal{N}QS_{tx}}$. Specifically, the average interarrival time for headers, payload fragments and last fragments is represented by $\mu_H = \frac{D}{\mathcal{N}QN}$, $\mu_F = \frac{D}{\mathcal{N}Q(S_{tx}-N-1)}$, and $\mu_L = \frac{D}{Q\mathcal{N}}$, respectively. Let t_1 denote the starting time of the first packet and the timestamps of the subsequent packets be given by $t_{i+1} = t_i + \sum_{i=1}^{n-1} A(i)$, where $A(i) = t_{i+1} - t_i$ is interarrival time of the two subsequent packets. As illustrated in Fig. 3, during an LR-FHSS packet an end-device changes the OBW frequency channels multiple times. We denote these moments $\tau_{i,j} = \{\tau_{i,1}, \tau_{i,2}, \ldots, \tau_{i,S_{tx}}\}$, where j denotes the hop within a packet, $j = 1, 2, 3 \ldots, S_{tx}$. The timestamp of each hop is thus given by:

$$\tau_{i,j} = \begin{cases} t_i + (j-1)\,T_H & j \le N \\ t_i + NT_H + T_W + (j-N-1)\,T_F & N+1 \le j \le S_{tx} \end{cases} \tag{3}$$

We consider that since LR-FHSS uses ALOHA-like channel access protocol, if two or more packets elements collide, the reception of these elements on the gateway can fail. Note, that LR-FHSS imply frequency hoping and end-device splits data into S_{tx} elements comprising headers and data fragments which have different transmission durations, which we denote T_H, T_F, and $T_{F_{last}}$. Therefore, to accurately model this, in the current study we present the collision model for the LR-FHSS which separately accounts the number of colliding packet elements for the transmission of a header, data fragment and the last fragment. The vulnerable times for LR-FHSS are illustrated in Fig. 4. Thus, the average number of packet elements arrivals during a target header's vulnerable interval $(\tau_{i,j} - T_H; \tau_{i,j} + T_H)$, for $j = 1, \ldots, N$ is defined as

$$A_H = \mu_H 2T_H + \mu_F(T_H + T_F) + \mu_L\big(T_H + T_{F_{last}}\big). \tag{4}$$

where $T_{F_{last}}$ is the duration of the last fragment. Let T_{PHY} be the on-air time required to transfer payload data fragments $(S_{tx} - N)$ and the duration of the last fragment be $T_{F_{last}} = T_{PHY} \pmod{T_F}$ which can differ from T_F. The average number of uplink packet elements transmitted in the interval

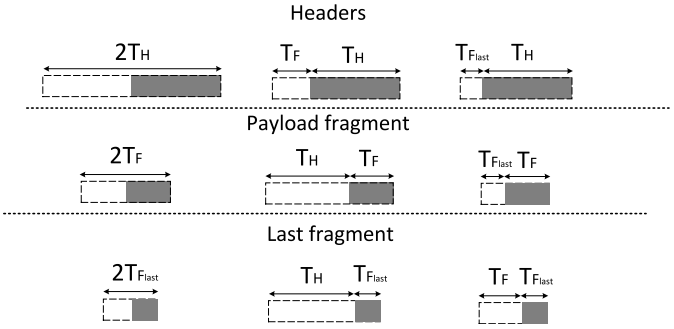

Fig. 4. Vulnerable times for LR-FHSS scheme.

$(\tau_{i,j} - T_F; \tau_{i,j+T_F})$, for $j = N+1, \ldots, S_{tx} - 1$ is thus given by

$$A_F = \mu_F 2T_F + \mu_H(T_H + T_F) + \mu_L\big(T_F + T_{F_{last}}\big). \tag{5}$$

Similarly, A_L, which denotes the average number of packet elements transmitted during the last fragment interval, is

$$A_L = \mu_L 2T_{F_{last}} + \mu_H(T_H + T_{F_{last}}) + \mu_F(T_F + T_{F_{last}}). \tag{6}$$

Let us focus on a single end-device and investigate the uplink performance under the co-channel interference caused by simultaneous transmissions. The overall success probability is composed of two components: $P_S = P_H(N)P_F(\gamma)$. The $P_H(N)$ represents the probability of successfully receiving at least one of N transmitted header replicas, thus

$$P_H(N) = 1 - \left(1 - \left(\frac{C-1}{C}\right)^{A_H - 1}\right)^N, \tag{7}$$

where $C = 280$ denotes the number of non-overlapping OBW frequency channels for DR8/DR9 and A_H is given by (4). The $P_F(\gamma)$, denotes the probability of correctly decoding more than γ broadcasted payload fragments as

$$P_F(\gamma) = \Pr[F_{rx} \ge \gamma] = 1 - \sum_{k=1}^{\gamma-1} \Pr[F_{rx} = k] \tag{8}$$

$$\Pr[F_{rx} = k] = \binom{F_{tx}}{k} p_F^k (1 - p_F)^{F_{tx} - k} \tag{9}$$

where F_{tx} denotes the number of transmitted physical payload fragments, F_{rx} is the number of received fragments. Note that $T_{F_{last}}$ can differ from T_F, which requires us to determine the average success probability of a single data fragment separately. Overall, p_F is the average success probability[1] of a single data fragment and it is given as

$$p_F = \frac{(F_{tx} - 1)\left(\frac{C-1}{C}\right)^{A_F - 1} + \left(\frac{C-1}{C}\right)^{A_L - 1}}{F_{tx}}, \tag{10}$$

B. Simulator Model

To validate the analytic models and enable more complex scenarios, which can be hard to approach analytically, we

[1]To account the difference in T_F and $T_{F_{last}}$, we calculate the average overall success probability (p_F) of a single data fragment which takes the average of the probabilities of the first $F_{tx} - 1$ payload fragments and the last fragment.

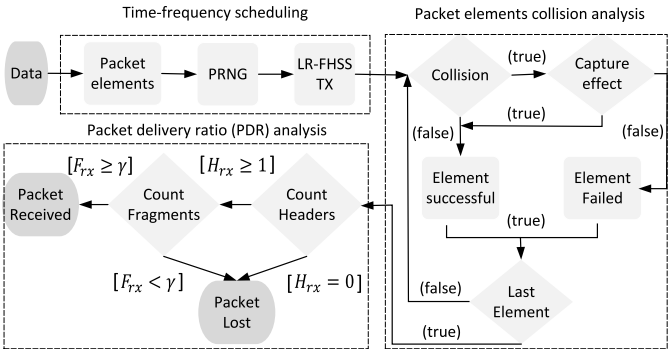

Fig. 5. System diagram of LR-FHSS simulator.

have also developed a MATLAB-based Monte Carlo simulation model for LR-FHSS (available, along with further details about its design and operation, from GitHub via [15]).

Note that in our simulations, we also account satellite's mobility at 7.4 km/s speed, which results in a rapid change of the distance between the gateway and the on-ground devices. This distance is given by [7], [8]:

$$d = R\left(\sqrt{\left(\frac{H+R}{R}\right)^2 - \cos^2(E)} - \sin(E)\right). \quad (11)$$

where $H = 780$ km denotes the orbital height of a satellite, $R = 6378$ km is Earth's radius, E is elevation angle in degrees defined as $E = \sin^{-1}(\frac{H(H+2R)-d^2}{2dR})$.

The rapid variation in elevation angle results in fluctuation of the channel characteristics. To reflect this fact in model, we account for the temporal change of the Rician fading effect $g = \sqrt{\frac{\kappa}{\kappa+1}}h_{LOS} + \sqrt{\frac{1}{\kappa+1}}h_{NLOS}$ with dynamic Rician factor (κ) as a function of E, as in [11]. Note that we imply that LR-FHSS receiver sensitivity is equivalent or higher than that of LoRa spreading factor 12 received, as discussed in [12]. A collision occurs when two or more end-devices transmit simultaneously in the same OBW channel. The capture effect, i.e., the possibility of a LoRaWAN gateway to receive the strongest packet element under interference from weaker signals is accounted through parameter δ and the probability of correct reception of a packet element is thus given by

$$P_{SIR} = \Pr\left[\frac{P_{tx}\,G_t\,G_r\,PL(d)|g|^2}{\sum P_{tx}\,G_t\,G_r\,PL(d_l)|g_l|^2} \geq \delta\right], \quad (12)$$

where δ is a power threshold, $PL(d)$ is free-space path loss, l are the indexes of interfering nodes, $G_r = 22.6$ dBi is directive antenna gain of a satellite-based non-terrestrial gateway and $G_t = 2.15$ dBi is the omnidirectional antenna gain of the ground LoRaWAN nodes [7], [8], [13]. The simulator allows to model the different distributions of the nodes and traffic patterns, and generates the time-frequency resource allocation pattern in accordance with LR-FHSS specification, from which the decision on whether the packet elements and the packet as whole are correctly received is made. The structural diagram and sequence of simulator's operation are illustrated in Fig. 5.

TABLE I
KEY MODELS' PARAMETERS

Parameters	Values
Carrier frequency (f_C)	868 MHz
OCW Channel	1
OCW Bandwidth (B)	137 kHz
DR8/DR9 OBW Channels (C)	280
DR8/DR9 OBW Channels/node	35
OBW minimum separation	3.9 kHz
Header replicas (N)	DR8 = 3, DR9 = 2
Coding rate (CR)	DR8 = $\frac{1}{3}$, DR9 = $\frac{2}{3}$
Header replica duration (T_H)	233 ms
Fragment duration (T_F)	50 ms
Transmit power (P_{tx})	14 dBm
Receiver Sensitivity	-137 dBm
Antenna gains	G_t = 2.15 dBi, G_r = 22.6 dBi
Path loss exponent (η)	2
Power threshold (δ)	6 dB
Nodes ($\mathcal{N}$)	0-300k
PHY payload (L)	10 bytes
Report period (Q)	900 s
Elevation angles (E)	$10^\circ \leq E \leq 90^\circ$
Rician Factor (κ)	$1.24 \leq \kappa \leq 25.11$
Orbital height (H)	780 km
Earth Radius (R)	6378 km

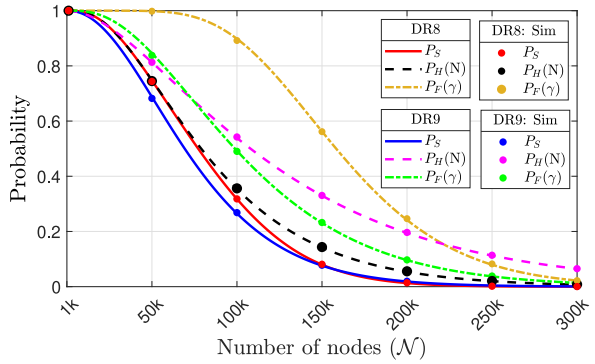

Fig. 6. The average probability of packet delivery P_S and its components: headers success probability ($P_H(N)$) and probability of enough payload fragments reception exceeding the threshold $P_F(\gamma)$ implying $\mathcal{Q} = 4$.

IV. SELECTED RESULTS

Table I lists the key parameters used for our simulations and analyses. Note that each point on the charts for simulation results is an average of 10^5 (i.e., 100k) random realizations of nodes' distributions and traffic patterns.

Figure 6 depicts the success probability for the packet delivery P_S, as well as that for headers $P_H(N)$ and the necessary number of data fragments $P_F(\gamma)$ as a function of the number of nodes $\mathcal{N}$ obtained analytically and via simulations. One can see that the analytical results match well the ones obtained through simulations. From the presented results, one can see that when $\mathcal{N}$ is below 150k the P_S for nodes operating with DR8 is higher than that using DR9. However, for denser network DR9 slightly outperforms DR8.

Notice that P_S for DR8 is dominated by $P_H(N)$ while $P_F(\gamma)$ degrades much slower than $P_H(N)$. For DR9, featuring lower header repetitions but a higher coding rate for payload fragments, the $P_H(N)$ is higher than that for DR8. The $P_F(\gamma)$, for DR9, however, stays below that for DR8 owing

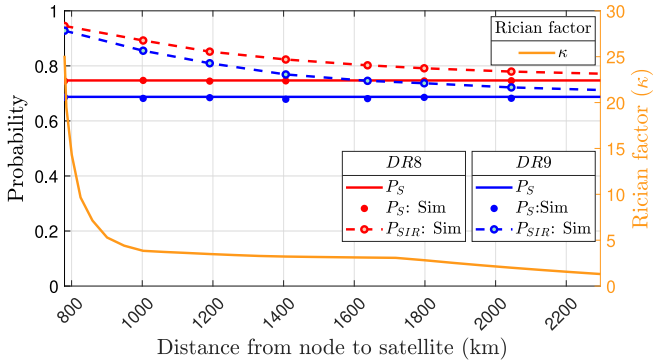

Fig. 7. The average probabilities as a complement of overall success probability P_S and P_{SIR} as function of distance from a node to satellite implying $\mathcal{N} = 50$ k and $Q = 4$. The right axis illustrates the change of the κ as a function of distance implied for simulations.

to a higher decoding threshold (γ). Specifically, the P_S for DR8 and DR9 is around 74.35% and 68.22%, respectively, at $\mathcal{N} = 50$ k. Furthermore, one can see that the P_S of both data rates gradually declines to 8.11% when the $\mathcal{N}$ reaches 150k. For the maximum number of nodes considered, P_S drops to 0.02% for both data rates. Figure 7 illustrates the overall success probability as a function of the distance between a ground node and the satellite for the case of $\mathcal{N} = 50$ k. Note that DR8 demonstrates the best performance, allowing a LoRaWAN node's packet to reach the satellite with P_S about 74.70%. With DR9, the P_S drops to 68.74% owing to the change in code rate from $\frac{1}{3}$ to $\frac{2}{3}$. Additionally, Fig. 7 demonstrates the P_{SIR}.[2] Moreover, since very limited information is currently available about the capture effect for LR-FHSS, we imply that to be demodulated correctly the target signal needs to be at least $\delta = 6$ dB stronger than the sum of the interfering ones, as in legacy LoRa [14]. The P_{SIR} curve for DR8 shows that the gateway can successfully receive a packet with probability exceeding 85.17% until the distance to a satellite reaches 1200 km. However, this probability declines to 77.16% at the highest distance. With DR9, the P_{SIR} stays above 75% within 1600 km from satellite and drops below 71.22% when the distance touches the coverage border. One can see that the capture effect boosted the average success probability (P_S) by 8.5% and 9.7% for DR8 and DR9, respectively. The right y axis is used to illustrate the time-varying characteristics of κ as a function of d.

V. Conclusion

To the best of our knowledge, the current letter is one of the first publications focusing on the newly-introduced in LoRaWAN LR-FHSS modulation-coding scheme, which is particularly promising for DtS mMTC. In this letter, we first developed analytical and simulation models characterizing the packet delivery of LR-FHSS and then used these to investigate the scalability of LR-FHSS networks. Our results show that LR-FHSS can support large-scale DtS networks of infrequently (once in fifteen minutes) reporting devices. Notably, our results reveal that for both data rates standardized in the EU the primary reason for packet loss is the loss of the headers and that the capture effect can notably boost the performance.

Note that technical information about LR-FHSS is today limited, and thus the presented results should be re-validated and detailed by the follow-up studies, especially the experimental ones. We hope that this letter will motivate future research, experimentation, and development of solutions involving LR-FHSS. In such a case, analyzing the co-existence of LoRa and LR-FHSS and terrestrial and non-terrestrial networks can be a perspective research direction. Among the other notable research directions are the study of the effects which the Doppler shift, satellite constellation design and more accurate modeling of satellites mobility, and multi-connectivity will have on the network performance.

[2]The probability of packet delivery accounting for packet recovery due to the capture effect is determined numerically via simulations, since there is no tractable closed-form solution to a linear combination of non-central χ^2 random variables nor of its ratio.

References

[1] "RP2-1.0.2 LoRaWAN® Regional Parameters." LoRa Alliance. [Online]. Available: https://lora-alliance.org/resource_hub/rp2-102-lorawan-regional-parameters/ (Accessed: Jun. 21, 2021).

[2] "LoRaWAN® Protocol Expands Network Capacity with New Long Range–Frequency Hopping Spread Spectrum Technology." Semtech. [Online]. Available: https://blog.semtech.com/lorawan-protocol-expands-network-capacity-with-new-long-range-frequency-hopping-spread-spectrum-technology (Accessed: Jun. 21, 2021).

[3] Z. Lin, M. Lin, T. de Cola, J.-B. Wang, W.-P. Zhu, and J. Cheng, "Supporting IoT with rate-splitting multiple access in satellite and aerial-integrated networks," *IEEE Internet Things J.*, vol. 8, no. 14, pp. 11123–11134, Jul. 2021.

[4] Z. Lin, M. Lin, B. Champagne, W.-P. Zhu, and N. Al-Dhahir, "Secure and energy efficient transmission for RSMA-based cognitive satellite-terrestrial networks," *IEEE Wireless Commun. Let.*, vol. 10, no. 2, pp. 251–255, Feb. 2021.

[5] J. A. Fraire, S. Céspedes, and N. Accettura, "Direct-to-satellite IoT—A survey of the state of the art and future research perspectives: Backhauling the IoT through LEO satellites," in *Proc. Ad-Hoc Mobile Wireless Netw. Conf.*, 2019, pp. 241–258.

[6] M. Centenaro, C. E. Costa, F. Granelli, C. Sacchi, and L. Vangelist, "A survey on technologies, standards and open challenges in satellite IoT," *IEEE Commun. Surveys Tuts.*, vol. 23, no. 3, pp. 1693–1720, 3rd Quart., 2021.

[7] M. Asad Ullah, K. Mikhaylov, and H. Alves, "Massive machine-type communication and satellite integration for remote areas," *IEEE Wireless Commun.*, vol. 28, no. 4, pp. 74–80, Aug. 2021.

[8] M. Asad Ullah, K. Mikhaylov, and H. Alves, "Enabling mMTC in remote areas: LoRaWAN and LEO satellite integration for offshore wind farms monitoring," *IEEE Trans. Ind. Informat.*, early access, Sep. 14, 2021, doi: 10.1109/TII.2021.3112386.

[9] G. Boquet, P. Tuset-Peiró, F. Adelantado, T. Watteyne, and X. Vilajosana, "LR-FHSS: Overview and performance analysis," *IEEE Commun. Mag.*, vol. 59, no. 3, pp. 30–36, Mar. 2021.

[10] "Semtech and EchoStar Mobile to Test Satellite IoT Connectivity Service Integrated With LoRaWAN®." Semtech. [Online]. Available: https://www.semtech.com/company/press/semtech-and-echostar-mobile-to-test-satellite-iot-connectivity-service-integrated-with-lorawan (Accessed: Jun. 21, 2021).

[11] J. Kim, C.-Y. Yang, and J. S. Jang, "Performance analysis of low-earth-orbit (LEO) mobile-satellite system using moment-based approximation of degradation factors," *IEEE Trans. Veh. Technol.*, vol. 55, no. 3, pp. 876–886, May 2006.

[12] Semtech Corporation, *LoRaWAN® Outer Space and High Capacity (Satellite)—The Things Conference 2021*. Accessed: Oct. 18, 2021. [Online Video]. Available: https://www.youtube.com/watch?v=xNNIXwPB_tw

[13] "Satellite earth stations (SES); possible European standardisation of certain aspects of satellite personal communications networks (S-PCN) phase 1 report," ETSI, Sophia Antipolis, France, Rep. ETR 093, 1993.

[14] J. M. de Souza Sant'Ana, A. Hoeller, R. D. Souza, H. Alves, and S. Montejo-Sánchez, "LoRa performance analysis with superposed signal decoding," *IEEE Wireless Commun. Let.*, vol. 9, no. 11, pp. 1865–1868, Nov. 2020.

[15] M. Asad Ullah. "Analysis-and-Simulation-of-LoRaWAN-LR-FHSS." GitHub. [Online]. Available: https://github.com/MuhammadAsadUllah1/Analysis-and-Simulation-of-LoRaWAN-LR-FHSS.git (Accessed: Dec. 12, 2021).